Title

INJECTION AND FALLOFF TEST ANALYSIS TO ESTIMATE PROPERTIES OF UNSATURATED FRACTORES

Permalink

https://escholarship.org/uc/item/00m0d743

Authors

Mishra, S.
Bodvarsson, G.S.
Attanayake, M.P.

Publication Date

1986-12-01

Lawrence Berkeley Laboratory
UNIVERSITY OF CALIFORNIA

EARTH SCIENCES DIVISION

Presented at the American Geophysical Union Fall Meeting,
San Francisco, CA, December 8–12, 1986

Injection and Falloff Test Analysis to Estimate Properties of Unsaturated Fractures

S. Mishra, G.S. Bodvarsson, and M.P. Attanayake

December 1986

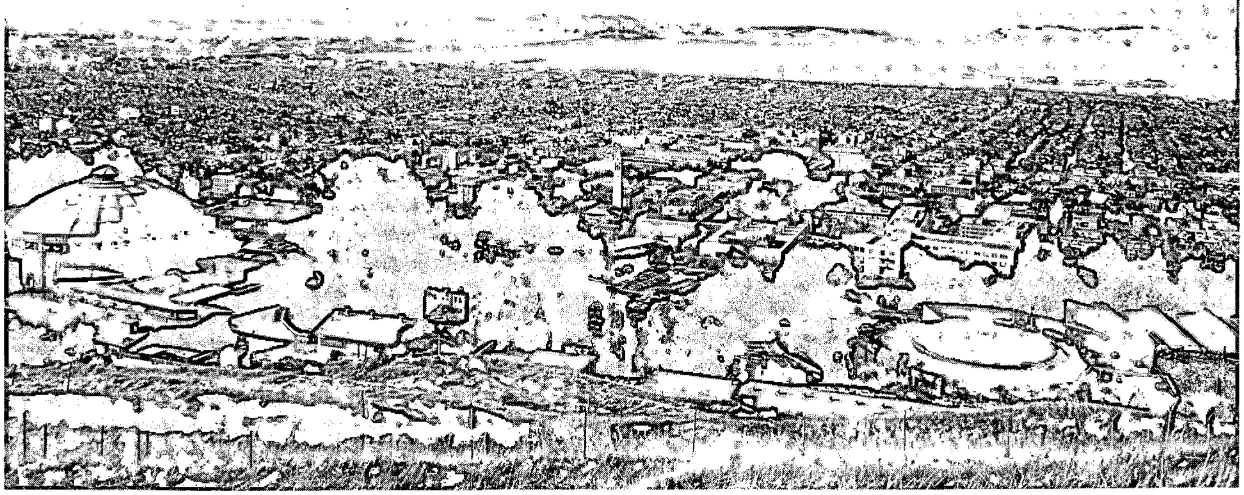

Prepared for the U.S. Department of Energy under Contract DE-AC03-76SF00098

INJECTION AND FALLOFF TEST ANALYSIS TO ESTIMATE PROPERTIES OF UNSATURATED FRACTURES

S. Mishra, G. S. Bodvarsson, and M. P. Attanayake

Earth Sciences Division, Lawrence Berkeley Laboratory
University of California, Berkeley, California 94720

Abstract. A new technique for calculating hydraulic properties of unsaturated fractured formations is proposed as an alternative to the common approach involving steady-state analysis of multi-rate gas injection tests. This method is based on graphical analysis of transient pressure data from an injection-falloff test sequence. Flow in a fracture of limited lateral extent, bounded above and below by an impermeable matrix, and intersected by a cylindrical borehole is described by two analytical models. The first model corresponds to early-time infinite acting radial flow, and the second to late-time linear flow. Interpretive equations are derived for computing fracture conductivity and volumetric aperture from early-time data, and fracture width from late-time data. Effects of fracture inclination and gravity are studied numerically, and found to be practically negligible for gas as well as water injection. Analysis of simulated injection-falloff tests using the suggested procedure yields results that agree well with simulator input values.

Introduction

Hydraulic properties of fractures such as conductivity and aperture are usually measured in an indirect manner. A common approach involves injecting gas into a packed-off section of a borehole which intersects the fractures(s) of interest. Gas is injected at a series of flow rates, and the stabilized pressure corresponding to each rate is measured. Permeability (or equivalently, hydraulic conductivity) is calculated from the appropriate steady-state solution of the pressure diffusion equation (Montazer, 1982; Trautz, 1984). Such a solution typically relates mass rate q_m to the pressure drop Δp^2 between the injection borehole and some observation point through a constant of proportionality which includes conductivity.

Montazer (1982) conducted an extensive experimental study of in-situ permeability measurements using such techniques, and identified three major effects which affect injection test response. These are (a) the Klinkenberg effect (Klinkenberg, 1941), (b) interference effects, and (c) the unsaturated nature of the rock. The Klinkenberg effect refers to slippage between gas molecules and pore walls at low pressures, which results in an apparent increase in permeability. This pressure dependence can be accounted for by measuring permeability at a range of pressures, and then extrapolating the linear pressure-permeability trend to infinite pressure so as to obtain the absolute (liquid) permeability. Montazer (1982) also observed that the pressure-permeability relationship may exhibit non-linearities because pressure gradients from one rate may interfere with new gradients which are created when rates are changed. These may be compounded by capillary and slip effects, which arise due to unsaturated conditions in the fracture.

Trautz (1984) used steady-state gas injection tests to measure gas conductivities of fractures in an unsaturated igneous rock. He developed equations for computing permeability from flow tests in elliptical flow situations, which are created when planar inclined fractures intersect vertical cylindrical boreholes. He observed that non-linear effects may arise under unsaturated conditions because of water blockage.

In this study, we explore the alternative approach of using transient pressure data from injection and falloff tests. This method involves injecting a fluid into the formation for a period of time, and then shutting the borehole to allow pressure to falloff. Graphical analysis of pressure-time data yields formation permeability, distance to linear barriers (e.g., lateral fracture boundaries) and formation pressure at initial conditions. Such techniques have been used for estimating hydraulic properties of saturated groundwater aquifers (Witherspoon et al., 1967), oil and gas reservoirs (Earlougher, 1977) and geothermal systems (Grant et al., 1982).

There are several advantages of using transient testing methods when compared to steady-state techniques. A steady-state test has to be conducted at several rates, and care has to be taken so that non-linear effects do not dominate the test when rates are changed. The onset of stabilization (i.e., steady-state conditions) can only be estimated crudely. Moreover, geometrical parameters such as volumetric (tracer) aperture and fracture width cannot be estimated from steady-state testing alone.

It is important to distinguish between the hydraulic aperture h and the volumetric aperture h_{vol}. The former is estimated from a relationship between permeability or permeability-thickness and aperture, (see Appendix C).

$$kh = 8.3 \times 10^6 h^3 \tag{1}$$

whereas the volumetric aperture is obtained from material balance

$$qt = \pi r^2 \Delta s \phi h_{vol} \tag{2}$$

If the fracture is visualized as a system containing several sections of varying apertures, the hydraulic aperture can be thought of as a parameter representing the effective conductance, whereas the volumetric aperture represents the average pore space for fluid flow.

This paper deals with the development of analytical models which describe pressure behavior in unsaturated fractures during injection-falloff testing. Interpretive equations are derived for computing fracture properties from analysis of pressure-time data. Effects of fracture inclination and gravity are investigated. Example analysis of a simulated injection-falloff test is shown.

Mathematical Model

In this section we describe the physical system of interest, and state the assumptions made in formulating the mathematical model. Based on the solution to this model, we then derive equations for analyzing injection and falloff pressure data. The basic premises of this discussion are as follows.

(a) Flow takes place in a plane horizontal fracture intersected by a cylindrical borehole (Fig. 1).

(b) The fracture has constant width and aperture, and is bounded above and below by an impermeable matrix.

(c) Initially, the fracture is unsaturated, i.e., it contains a two-phase mixture of air and water. Following Perrine (1956), we assume that single-phase flow equations can be used to describe two-phase flow if total mobility (sum of individual phase mobilities) is substituted for single-phase mobility, where mobility $\lambda = k/\mu$.

(d) During injection, the injected fluid displaces the formation fluids in a piston-like manner and a sharp moving front develops in the system, the presence of which creates a mobility contrast between the inner (invaded) and outer (uninvaded) zones.

(e) The front moves at a constant areal velocity during injection, and is stationary during pressure falloff.

(f) Wellbore storage and skin effects are neglected.

It is useful to conceptualize the temporal development of flow in the fracture during injection. At early times, before either the pressure or the saturation front has reached the lateral boundaries of the fracture, flow will be radial. Once the effects of the lateral boundaries have been felt, the flow regime will change from radial to linear. At late times, the borehole will behave like a plane source and both pressure and saturation fronts will move in a linear fashion (see Fig. 1(b)). This suggests that early-time radial flow and later-time linear flow solutions may be superimposed to describe the flow behavior approximately. Derivations are given for the case of ideal gas injection, and can easily be extended to liquid systems. An average pressure $\overline{p}$ is used for converting derivatives of p to derivatives of p^2 so that the flow equations are linearized. It should be pointed out that the p^2 formulation limits the applicability of this model to small pressure changes, so that the equations are linearized. This point is discussed in greater detail in Mishra et al. (1987).

Appendices A and B outline the mathematical formulation of the moving front problem during the radial and linear flow periods respectively, as well as analytical solutions. In this section, we present the interpretive equations for analyzing transient injection-falloff test data.

Interpretive equations

During the early part of injection, when flow is still radial, the injection pressure response is given by

$$p_{wf}^2 - p_i^2 = \frac{1.151 q \overline{p}}{\pi \lambda_1 h} \left(\log \frac{t}{r_w^2} + \log \eta_1 + \frac{S + .405}{1.151} \right) \quad (3)$$

Eq. (3) suggests that a graph of injection pressure squared p_{wf}^2 against the logarithm of injection time t should yield a straight line with slope inversely proportional to the mobility-thickness of the invaded zone $\lambda_1 h$. The early falloff pressure response is given by

$$p_{ws}^2 - p_i^2 = \frac{1.151q\overline{p}}{\pi\lambda_1 h}\left(\log\frac{t_p+\Delta t}{\Delta t} + \frac{S}{1.151}\right) \qquad (4)$$

Eq. (4) indicates that a graph of the early falloff pressure squared p_{ws}^2 against the logarithm of the time ratio $(t_p+\Delta t/\Delta t)$ should also produce a straight line with slope inversely proportional to $\lambda_1 h$. The hydraulic aperture can be obtained from the cubic law, Eq. (1). The pressure response during the middle falloff period is given by

$$p_{ws}^2 - p_i^2 = \frac{1.151q\overline{p}}{\pi\lambda_2 h}\left(\log\frac{t_p+\Delta t}{\Delta t}\right) \qquad (5)$$

which implies that a graph of p_{ws}^2 against log $(t_p+\Delta t)/\Delta t$ should now produce a straight line with slope inversely proportional to the mobility-thickness of the uninvaded (in-situ) zone $\lambda_2 h$. The late time injection pressure response is given by

$$p_{wf}^2 - p_i^2 = \frac{1.128q\overline{p}}{\lambda_2 bh}\sqrt{\eta_2^t} \qquad (6a)$$

from which, by superposition, the late time fall off response is given by

$$p_{ws}^2 - p_i^2 = \frac{1.128q\overline{p}}{\lambda_2 bh}\sqrt{\eta_2}\left(\sqrt{t_p+\Delta t} - \sqrt{\Delta t}\right) \qquad (6b)$$

which suggests that a cartesian graph of p_{ws}^2 against the time group $(\sqrt{t_p+\Delta t} - \sqrt{\Delta t})$ should produce a straight line with slope inversely proportional to the fracture width b.

As indicated above, Eq. (3) through (6) present a simple method for estimating the conductivities of the invaded and uninvaded zones, the hydraulic aperture and the fracture width. Under ideal conditions, it might be possible to estimate the volumetric (tracer) aperture, a scheme for which is given below.

Let $p_{wf}^2|^*$ be the injection pressure squared when $t/r_w^2 = 1$, and let $p_{ws}^2|^*$ the falloff pressure squared when $(t_p+\Delta t)/\Delta t=1$. Then from Eq. (3) and (4), one obtains after some manipulations

$$\log \eta_1 = \frac{(p_{wf}^2|^* - p_{ws}^2|^* - 0.352\ m)}{m} \qquad (7)$$

where m is the slope of the early-time injection (or falloff) pressure-time data

$$m = \frac{1.151 q \overline{p}}{\pi \lambda_1 h} \tag{8}$$

Then the volumetric aperture is given by

$$h_{vol} = \frac{q}{(\pi a \phi \Delta s \eta_1)} \tag{9}$$

based on the definition of the dimensionless front velocity group a, as given in Appendix A. By considering the validity of the log-approximation to the Ei-integral during the early falloff period, it can be shown that (Mishra et al., 1987) the dimensionless group a is approximately represented by

$$a \approx \frac{6}{\{\frac{(t_p + \Delta t)}{\Delta t}\}^{**}} \tag{10}$$

with the denominator being the time group at which the semi-log straight line on the early-time falloff graph ends.

Effects of Fracture Inclination

When flow in an inclined fracture is modelled, two additional factors need to be considered. Because of the altered flow geometry (cylindrical borehole and inclined fracture), early-time flow may no longer be radial. Moreover, the influence of gravity forces vis-a-vis viscous forces has to be taken into account. These effects are discussed below.

Modifications in flow geometry

When an inclined fracture is intersected by a cylindrical borehole, the resulting conic section is an ellipse, and the flow geometry is elliptical rather than radial. Trautz (1984) derived steady-state elliptical flow solutions to compute gas conductivity in natural inclined fractures and used these to interpret data from field tests. In his extensive study on transient flow in elliptical systems, Kucuk (1978) showed that any elliptical flow system can be converted to an equivalent radial system beyond a certain dimensionless time t_{Dr}, which is graphed in Fig. 2 as a function of a/b. The pertinent terms are

$$\frac{a}{b} = \sec \alpha \qquad (11)$$

$$r_w' = r_w \tan \alpha \frac{(1+\frac{a}{b})}{(\frac{a}{b})^2-1} \qquad (12)$$

$$t_{Dr} = \frac{kt\overline{p}}{\phi\mu r_w^2} \qquad (13)$$

where a and b are the semi-major and semi-minor axes of the borehole ellipse, α is the fracture inclination from horizontal and r_w is the actual wellbore radius. For most practical cases, the onset of radial flow occurs at very early times. As an example, for the case of air injection, if $k = 5$ D, $\overline{p} = 1$ atm, $\phi = 0.50$, $r_w = 10$ cm,and $\alpha = 60°$, we have

$\frac{a}{b} = 2$; $t_{Dr} = 20$ (Fig. 2),

$r_w' = 15$ cm (Eq. 12),

$t \approx 8$ s (Eq. 13).

Thus, after about eight seconds of injection, the system will behave like a radial system for all practical purposes. Hence, it is reasonable to assume that elliptical flow effects can be modeled by radial flow equations at all times of interest.

Gravitational effects

In highly unsaturated inclined fractures, the initial (static) pressure distribution will be nearly uniform because of negligible gravitational potential of gas. Once injection begins, the fluid distribution can be approximated by

$$q = -\lambda_1 h \left(\frac{\partial p}{\partial(\ln r)} \pm \frac{\rho g r_w \sin \alpha}{1.0133 \times 10^6} \right) \qquad (14)$$

where the positive and negative signs refer to the injected fluid flux in up- and down-dip directions, respectively. For the case of gas injection, the gravitational component will usually be much smaller than the flow rate induced pressure gradient, since the density of gas is very small. This will result in almost equal amounts being injected updip and downdip, and consequently the effects of gravity on the pressure transient response will be negligible. For the case of water injection, the dynamic distribution of fluids in updip and downdip directions will depend on the relative magnitudes of the pressure gradient and the gravitational terms. Since the pressure gradient is affected by the injection rate, one would expect gravity effects to be dominant primarily at low rates (small pressure gradients). However, simulation results indicate that for thin fractures the flow rate induced pressure gradients are orders of magnitude higher than the gravitational term even at small injection rates (these are tabulated in Table 1). A practical implication of this observation is that errors in analyzing transient pressure data from inclined fractures using equations derived for horizontal fractures will usually be small.

Model Verification

Two simulated injection-falloff test sequences were analyzed using the methods developed in this study as a verification exercise. Pressure-time data for an air-injection and water-injection test were simulated using TOUGH (Pruess, 1985), a computer program for calculating two-phase flow of water and air. Results of the air-injection test analysis are briefly described here. Details of the simulation study and interpretation of the simulated water injection test may be found in Mishra et al. (1987).

Table 2 lists pertinent test data, rock and fluid properties used. The injection test data, early-time falloff data and late-time falloff data are graphed in Figure 3 through 5. The mobility-thickness of the inner (invaded) zone is obtained from the slope of linear portions of Fig. 3 or 4, and using Eq. (8) it is calculated to be 200 D-cm/cp. This compares well with the simulator input value of 210 D-cm/cp. From Eq. (7), the inner zone diffusivity η_1 is estimated to be 805 cm^2/s, as opposed to the actual value of 820 cm^2/s. The time ratio $((t_p + \Delta t)/\Delta t)^{**}$, at which the early-time semi-log straight line ends during falloff, from Figure 4 is $\approx$10.5, from which the volumetric aperture h_{vol} can be estimated to be 0.9 cm using Eq. (9). The actual value used is 1 cm. Finally, from the slope of the linear portion on the late-time falloff graph (Fig. 5), the fracture width b can be computed if the mobility-thickness and diffusivity corresponding to the outer zone are known. Since saturation changes are small (because of near-unity mobility ratio), these parameters can be assumed to be roughly equal to the inner zone values. The fracture width b can then be calculated from Eq. (6) as 9.6 m, which compares well with the input value of 10 m.

Discussion

It has been shown that the simple model proposed here for air injection test gives reasonable values for many parameters of interest in fractured unsaturated rocks. Results for water injection test although not shown here, were quite similar (Mishra, et al., 1987). In general, the case of water injection into an unsaturated fracture leads to a greater mobility contrast between the injected and in-situ fluids, and hence to a sharper moving front. Both inner and outer zone mobility-thicknesses are readily calculated from the two falloff semi-log straight lines. However, a knowledge of the outer zone diffussivity is required in order to estimate the fracture width. Another problem with water injection is that it might disturb the formation, which may be an important consideration if the ultimate objective is to use the formation as a nuclear waste repository.

A problem with gas (or air) injection is that the system response may be non-linear if pressure changes are not small. This requires a proper selection of the injection rate, so that pressure levels do not exceed 2-3 atmospheres. Another complication in test interpretation is the need to know the saturation changes in the invaded zone in order to estimate the volumetric aperture. Such information will usually not be available.

For thin fractures (which is commonly the case), even small injection rates will cause pressure gradients which are large compared to the gravitational terms. This is an important observation since it facilitates the use of horizontal fracture system equations to interpret pressure data from inclined fracture system. Another significant finding is that the duration of elliptical flow in inclined fracture-borehole geometry is very short, and hence early-time flow may be assumed to be purely radial.

Conclusions

(1) Analytical models for analyzing gas and water injection-falloff tests in unsaturated fractured formations have been developed. Interpretive equations to estimate fracture permeability, width and aperture form graphical analysis of transient pressure data have been derived.

(2) Effects of fracture inclination and gravity have been investigated numerically, and found to be negligible.

(3) The proposed method is an alternative to conventional multi-rate gas injection testing, and has the potential of providing information regarding geometrical characteristics such as fracture width and aperture.

Acknowledgements. The authors acknowledge valuable discussions with scientists from the Nuclear Hydrology Group of the U. S. Geological Survey in Denver, Colorado, especially Parviz Montazer and Dwight Hoxie. Technical review of this manuscript by Yvonne Tsang and Sally Benson of Lawrence Berkeley Laboratory is appreciated. This work was carried out under U.S. Department of Energy Contract No. DE-AC03-76SF00098 via the DOE-Nevada Office in cooperation with USGS-Denver; project direction provided by B. Wilson.

References

Earlougher, R. C., Jr., Advances in Well Test Analysis, Monograph 5, *Society of Petroleum Engineers,* Dallas, 1977.

Grant, M.A., I.G. Donaldson and P.F. Bixley, *Geothermal Reservoir Engineering,* Academic Press, New York City, 1982.

Klinkenberg, L. J., The Permeability of Porous Media to Liquids and Gases, *API Drill. and Prod. Prac.,* 200, 1941.

Kucuk, F., Transient Flow in Elliptical Systems, Ph.D. dissertation, Stanford University, Stanford, California, 1978.

Mishra, S., G. S. Bodvarsson, and M. P. Attanayake, Estimating Properties of Unsaturated Fractured Formations for Injection and Falloff Tests, Lawrence Berkeley Laboratory Report LBL-22102, Berkeley, California, 1987.

Montazer, P.M., Permeability of Unsaturated, Fractured Metamorphic Rocks Near an Underground Opening, Ph.D. thesis, Colorado School of Mines, Golden, Colorado, 1982.

Muskat, M., The Flow of Homogeneous Fluids through Porous Media, IHRDC, Boston, 1982.

Perrine, R.L., Analysis of Pressure Buildup Curves, API Drill and Prod. Prac., 482, 1956.

Pruess, K., TOUGH Users Guide, Lawrence Berkeley Laboratory Report LBL-20070, Berkeley, California, 1985.

Ramey, H.J., Jr., Approximate Solutions for Unsteady Liquid Flow in Composite Reservoirs, *J. Cdn. pet. Tech.*, January-March, pp. 32-37, 1970.

Trautz, R.C., Rock Fracture Aperture and Gas Conductivity Measurements In-Situ, Topical Report, Contract No. NRC-04-81-224, submitted to the U.S. Nuclear Regulatory Commission, 1984.

Witherspoon, P.A., I. Javandel, S.P. Neuman, and R.A. Freeze, Interpretation of Aquifer Gas Storage Conditions from Water Pumping Tests, Monograph on Project NS-38, American Gas Association, New York, 1967.

Woodward, D.K. and R.K.M. Thambynayagam, Pressure Buildup and Falloff Analysis of Water Injection Tests, unsolicited manuscript submitted to the Society of Petroleum Engineers, paper SPE-12344, 1983.

Nomenclature

a	front velocity ratio
b	fracture width (cm)
D	diffusivity ratio
h	hydraulic fracture aperture (cm)
h_{vol}	volumetric fracture aperture (cm)
k	permeability (Darcy)
m	semi-log straight line slope (atm/$\approx$)
M	mobility ratio
p_i	initial fracture pressure (atm)
p_{wf}	injection well flowing pressure (atm)
p_{ws}	injection well shut-in pressure (atm)
q	volumetric injection rate (cc/s)
q_m	mass injection rate (kg/s)
r	radial distance (cm)
r_w	wellbore radius (cm)
r_f	distance to front (radial flow) (cm)
Δs	saturation change in invaded zone
S_{wi}	initial water saturation
S_{gi}	initial gas saturation
t_p	injection time (sec)
Δt	shut-in time (sec)
x	linear distance (cm)
x_f	distance front (linear flow) (cm)

Greek Symbols

α	fracture inclination (degrees)
ρ	density (kg/cc)
ϕ	porosity
μ	viscosity (cp)
η	diffusivity (cm^2/s)
λ	mobility (darcy-cm/cp)
γ	constant, 1.780072

Other Expressions

Ei(-x)exponential integral, $Ei(-x) = -\int_x^{\infty} \frac{e^{-u}du}{u}$

Figures

Appendix A

Transient Pressure Response during Radial Flow

In this section, we present an analytical model describing the pressure response during the movement of a radial saturation front. Flow in the inner (invaded) and outer (uninvaded) zones is governed by the diffusivity equation

$$\frac{1}{r}\frac{\partial}{\partial r}\left(r\frac{\partial p_1^2}{\partial r}\right)=\frac{1}{\eta_1}\frac{\partial p_1^2}{\partial t} \tag{A.1a}$$

$$\frac{1}{r}\frac{\partial}{\partial r}\left(r\frac{\partial p_2^2}{\partial r}\right)=\frac{1}{\eta_2}\frac{\partial p_2^2}{\partial t} \tag{A.1b}$$

Here, subscripts 1 and 2 refer to the inner and outer zones respectively. Diffusivity η is defined as

$$\eta_{1,2}=\frac{\overline{p}\lambda_{1,2}}{\phi} \tag{A.2}$$

Initially, the system is in pressure equilibrium

$$p_1^2(r,0)=p_2^2(r,0)=p_i^2 \tag{A.3}$$

A line source well is injecting at a constant rate at the inner boundary

$$\frac{\pi\lambda_1 h}{\overline{p}}\left(r\frac{\partial p_1^2}{\partial r}\right)_{r\to 0}=q \tag{A.4}$$

The outer boundary is undisturbed at all times

$$p_2^2(\infty,t)=p_i^2 \tag{A.5}$$

At the moving front, both pressure and flux are continuous

$$p_1^2(r_f,t)=p_2^2(r_f,t) \tag{A.6}$$

$$\lambda_1\left(\frac{\partial p_1^2}{\partial r}\right)_{r_f}=\lambda_2\left(\frac{\partial p_2^2}{\partial r}\right)_{r_f} \tag{A.7}$$

The movement of the front is assumed to be piston-like, i.e., the front is modeled as a plane of constant saturation separating the injected fluid from the in-situ fluid. From material balance considerations

$$qt = \pi\, r_f^2\, h_{vol}\, \phi\, \Delta s \tag{A.8}$$

This implies that the movement of the front is such that r_f^2 / t is a constant.

Solution of this set of equations is obtained by the method of Boltzman transformation, details of which are presented elsewhere (Mishra et al., 1987). Similar solutions, for liquid flow in composite media, have been given by Ramey (1970) and Woodward and Thambynayagam (1983).

The general expressions for pressure response in the inner and outer zones are given by

$$p_1^2 - p_i^2 = \frac{q\bar{p}}{2\pi\lambda_1 h}\left\{ \mathrm{Ei}\left(-\frac{r^2}{4\eta_1 t}\right) - \mathrm{Ei}\left(-\frac{r_f^2}{4\eta_1 t}\right)\right\}$$

$$+ \frac{q\bar{p}}{2\pi\lambda_2 h}\exp\left\{-\left(\frac{r_f^2}{4\eta_1 t} - \frac{r_f^2}{4\eta_2 t}\right)\right\}\mathrm{Ei}\left(-\frac{r_f^2}{4\eta_2 t}\right) \tag{A.9}$$

$$p_2^2 - p_i^2 = + \frac{q\bar{p}}{2\pi\lambda_2 h}\exp\left\{-\left(\frac{r_f^2}{4\eta_1 t} - \frac{r_f^2}{4\eta_2 t}\right)\right\}\cdot \mathrm{Ei}\left(-\frac{r^2}{4\eta_2 t}\right) \tag{A.10}$$

Where Ei (-x) is the exponential integral defined as

$$\mathrm{Ei}(-x) = -\int_{u}^{\infty} \frac{e^{-u}}{u}\, du \tag{A.11}$$

The wellbore being the observation point of interest, one obtains

$$p_{wf}^2 - p_i^2 = \frac{q\bar{p}}{2\pi\lambda_1 h}\left\{ \mathrm{Ei}\left(-\frac{r_w^2}{4\eta_1 t}\right) - \mathrm{Ei}\left(-\frac{r_f^2}{4\eta_1 t}\right)\right\}$$

$$+ \frac{q\bar{p}}{2\pi\lambda_2 h}\cdot \exp\left\{-\left[\left(\frac{r_f^2}{4\eta_1 t}\right) - \left(\frac{r_f^2}{4\eta_2 t}\right)\right]\right\}\cdot \mathrm{Ei}\left(-\frac{r_f^2}{4\eta_2 t}\right) \tag{A.12}$$

Define

$$a = \frac{r_f^2}{\eta_1 t} = \frac{\left(\dfrac{q}{\pi h_{vol}\phi\Delta S}\right)}{\eta_1} ,$$

$$M = \frac{\lambda_1}{\lambda_2}$$

and

$$D = \frac{\eta_1}{\eta_2} \quad .$$

Eq. (A.12) can now be rewritten as

$$p_{wf}^2 - p_i^2 = \frac{q\bar{p}}{\pi\lambda_1 h}\left\{\frac{1}{2}\,\mathrm{Ei}\left[-\frac{r_w^2}{4\eta_1 t}\right] + \frac{M}{2}\cdot\exp\right.$$

$$\left.\left\{-\frac{a(1-D)}{4}\cdot\mathrm{Ei}\left[-\frac{aD}{4}\right] - \frac{1}{2}\,\mathrm{Ei}\left[-\frac{a}{4}\right]\right]\right\} \qquad \text{(A.13)}$$

For small arguments of the exponential integral, the log-approximation $\mathrm{Ei}(-x) = ln(\gamma x)$ has been shown to be valid even for small times at the wellbore (Earlougher, 1977). Using this identity for the first Ei-term, and defining a dimensionless skin factor due to the moving front

$$S = \frac{M}{2}\cdot\exp\left\{-\frac{a(1-D)}{4}\cdot\mathrm{Ei}\left(-\frac{aD}{4}\right\} - \frac{1}{2}\,\mathrm{Ei}\left[-\frac{a}{4}\right] \qquad \text{(A.14)}$$

one obtains from Eq. (A.13)

$$p_{wf}^2 - p_i^2 = \frac{q\bar{p}}{\pi\lambda_1 h}\left\{\frac{1}{2}\,ln\left[\frac{t}{r_w^2}\right] + \frac{1}{2}\,ln(\eta_1) + S + 0.405\right\} \qquad \text{(A.15)}$$

Eq. (3) of the text is now obtained directly by changing from ln to log. If injection is stopped after a time t_p, the falloff pressure response may be generated using the principle of superposition. The falloff pressure response may be defined as

$$p_{ws}^2(\Delta t) - p_i^2 = \left\{p_{wf}^2(t_p + \Delta t) - p_i^2\right\} - \left\{p_{wf}^2(\Delta t) - p_i^2\right\} \qquad \text{(A.16)}$$

Substituting from (A.12), and considering the early-falloff response, when $t_p >> \Delta t$, one can obtain Eq. (4) of the text after some manipulations. Similarly, Eq. (5), defining the pressure response during the middle-falloff period, can be derived. These derivations are described in detail in Mishra et al. (1987).

Appendix B

Pressure Transient Behavior for the Linear Flow Period

In this appendix, we present an analytical model describing the pressure response during the movement of a linear front. As in the radial flow case, the diffusivity equation governs flow in both the inner (invaded) and outer (uninvaded) zones:

$$\frac{\partial^2 p_j^2}{\partial x^2} = \frac{1}{\eta_j} \frac{\partial p_j^2}{\partial t} \quad j = 1,2 \tag{B.1}$$

Initially, the system is in pressure equilibrium:

$$p_1^2(x,0) = p_2^2(x,0) = p_i^2 \tag{B.2}$$

A plane source is injecting at a constant rate at the inner boundary:

$$\frac{\lambda_1 bh}{2\overline{p}} \frac{\partial p_1^2}{\partial x}\bigg|_{x\to 0} = -\frac{q}{2} \tag{B.3}$$

The outer boundary is undisturbed at all times:

$$p_2^2(\infty,t) = p_i^2 \tag{B.4}$$

At the moving boundary, both fluid flux and pressure are continuous:

$$\lambda_1 \frac{\partial p_1^2}{\partial x}\bigg|_{x_f} = \lambda_2 \frac{\partial p_2^2}{\partial x}\bigg|_{x_f} \tag{B.5}$$

$$p_1^2(x_f,t) = p_2^2(x_f,t) \tag{B.6}$$

The front moves as a plane, which is expressed by the material balance condition

$$qt = bx_f\, h_{vol}\, \phi\, \Delta s \tag{B.7}$$

These equations are converted into dimensionless form through the use of the following dimensionless variables.

$$p_D^* = \frac{\lambda_1 h}{q\overline{p}} (p^2 - p_i^2) \tag{B.8}$$

$$t_D^* = \eta_1 \left(\frac{t}{b^2}\right) \tag{B.9}$$

$$x_{fD} = \frac{x_f}{b} \tag{B.10}$$

$$x_D = \frac{x}{b} \tag{B.11}$$

$$m = \frac{\lambda_1}{\lambda_2} \tag{B.12}$$

$$D = \frac{\eta_1}{\eta_2} \tag{B.13}$$

The time-dependence from the dimensionless equations is eliminated through the use of the Laplace transformation

$$\overline{p}_D^* (x_D, l) = \int_0^{t_D^*} e^{-l\tau}\, p_D^* (x_D, \tau)\, d\tau \tag{B.14}$$

where l is the Laplace space parameter.

The dimensionless pressure $\overline{p}_{D1}^*$ and $\overline{p}_{D2}^*$ describing the pressure response in the inner and outer zones, in Laplace domain,

$$\overline{p}_{D1}^* = \frac{\left\{1 + \frac{M-\sqrt{D}}{M+\sqrt{D}} \cdot \exp\left(2x_D\sqrt{l}\,\right) \cdot \exp\left(-2x_{fD}\sqrt{l}\,\right)\right\}}{l^{3/2} \exp(x_D\sqrt{l}\,)\left\{1 - \frac{M-\sqrt{D}}{M+\sqrt{D}} \exp(-2x_{fD}\sqrt{l}\,)\right\}} \tag{B.15}$$

$$\overline{p}_{D2}^* =$$

$$\frac{2M\exp(x_{fD}\sqrt{lD})}{l^{3/2}\exp(x_D\sqrt{lD})\left\{(M+\sqrt{D})\exp(x_{fD}\sqrt{l}\,) - (M-\sqrt{D})\exp(-x_{fD}\sqrt{l}\,)\right\}} \tag{B.16}$$

See Mishra et al. (1987) for details. At the borehole (which is the primary observation point), Eq. (B.15) reduce to

$$\overline{p}_{D1}^*(x_D = 0) = \overline{p}_{wD}^* = \frac{\left\{1 + \frac{M-\sqrt{D}}{M+\sqrt{D}} \exp\left(-2x_{fD}\sqrt{l}\,\right)\right\}}{l^{3/2}\left\{1 - \frac{M-\sqrt{D}}{M+\sqrt{D}} \cdot \exp\left(-2x_{fD}\sqrt{l}\,\right)\right\}} \tag{B.17}$$

Since linear flow takes place only at late-times, it is useful to derive a long-time approximation from Eq. (B.17) This is given by

$$\lim_{l \to 0} \bar{p}^{*}_{wD} \approx \frac{1+\dfrac{M-\sqrt{D}}{M+\sqrt{D}}}{l^{3/2}\left\{1-\dfrac{M-\sqrt{D}}{M+\sqrt{D}}\right\}} = \frac{M}{l^{3/2}\sqrt{D}} \qquad \text{(B.18)}$$

Equation (B.38) is easily in inverted to yield

$$p^{*}_{wD}\,(t^{*}_{D}) = \frac{M}{\sqrt{D}} \cdot \frac{2}{\sqrt{\pi}} \cdot \sqrt{t^{*}_{D}} \qquad \text{(B.19)}$$

Substituting for the dimensionless variables, one obtains Eq. (6) of the text.

Appendix C

Relation between Fracture Permeability and Aperture

A relation between effective fracture permeability and aperture can be derived from hydrodynamical considerations (Muskat, 1982). A fracture of width h may be considered equivalent to an open linear channel of equal width for viscous flow conditions, the carrying capacity of such a linear channel, per unit pressure gradient, is given by

$$A = \frac{h^3}{12\mu} \tag{C.1}$$

where Q is the thruput and μ the viscosity. By equating this expression with Darcy's law, the equivalent permeability of the fracture, in cm^2, is given as

$$k = \frac{h^2}{12} \tag{C.2}$$

where h is in cm. Converting permeability to darcies, and multiplying both sides by h, one obtains

$$Kh = 8.3 \times 10^6\, h^3 \tag{C.3}$$

which is the same as Eq. (1) of the main text.

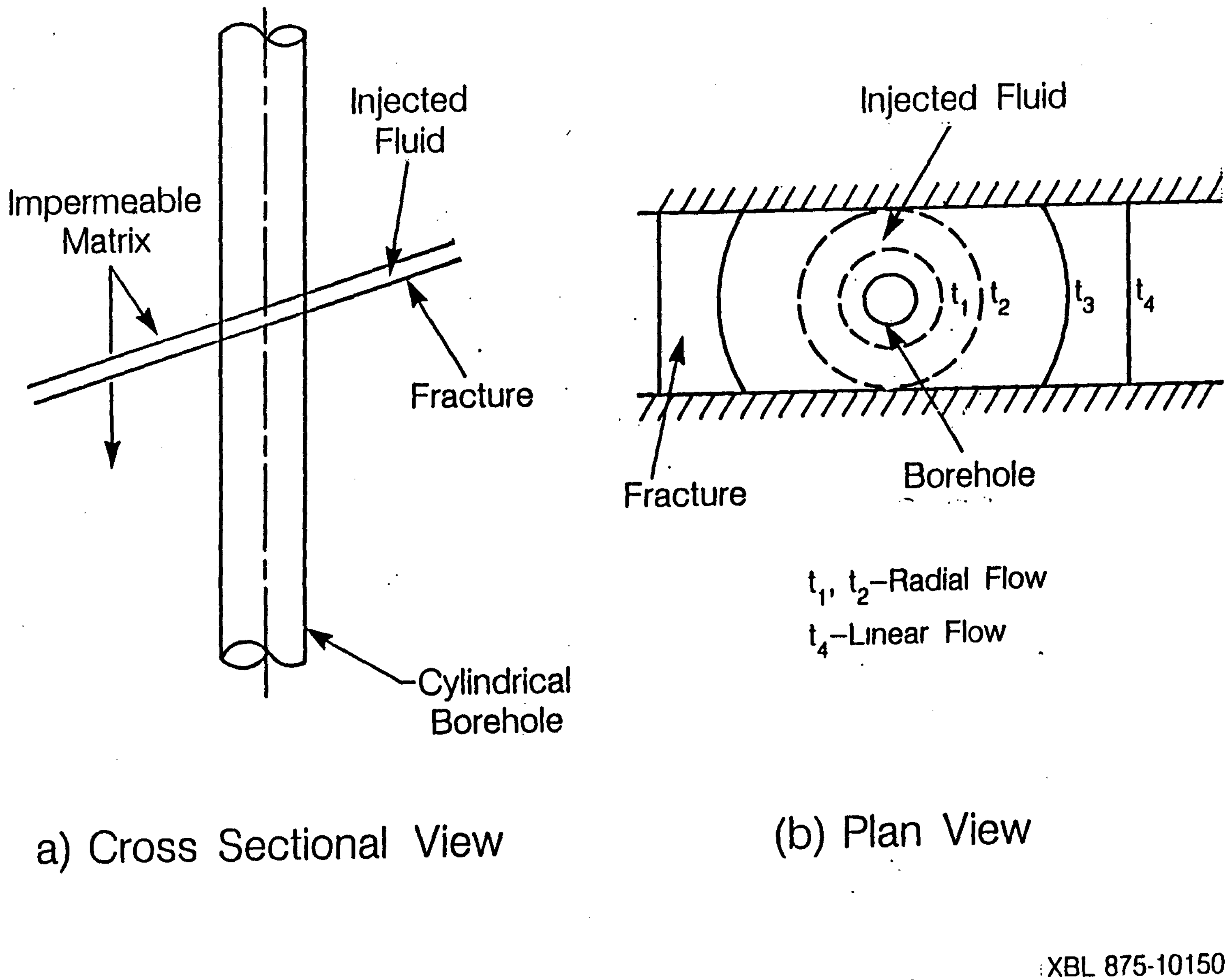

Fig. 1. Schematic of physical system: (a) cross-sectional view, of borehole intersecting an inclined fracture, (b) plan view illustrating a front moving away from the well in the fracture.

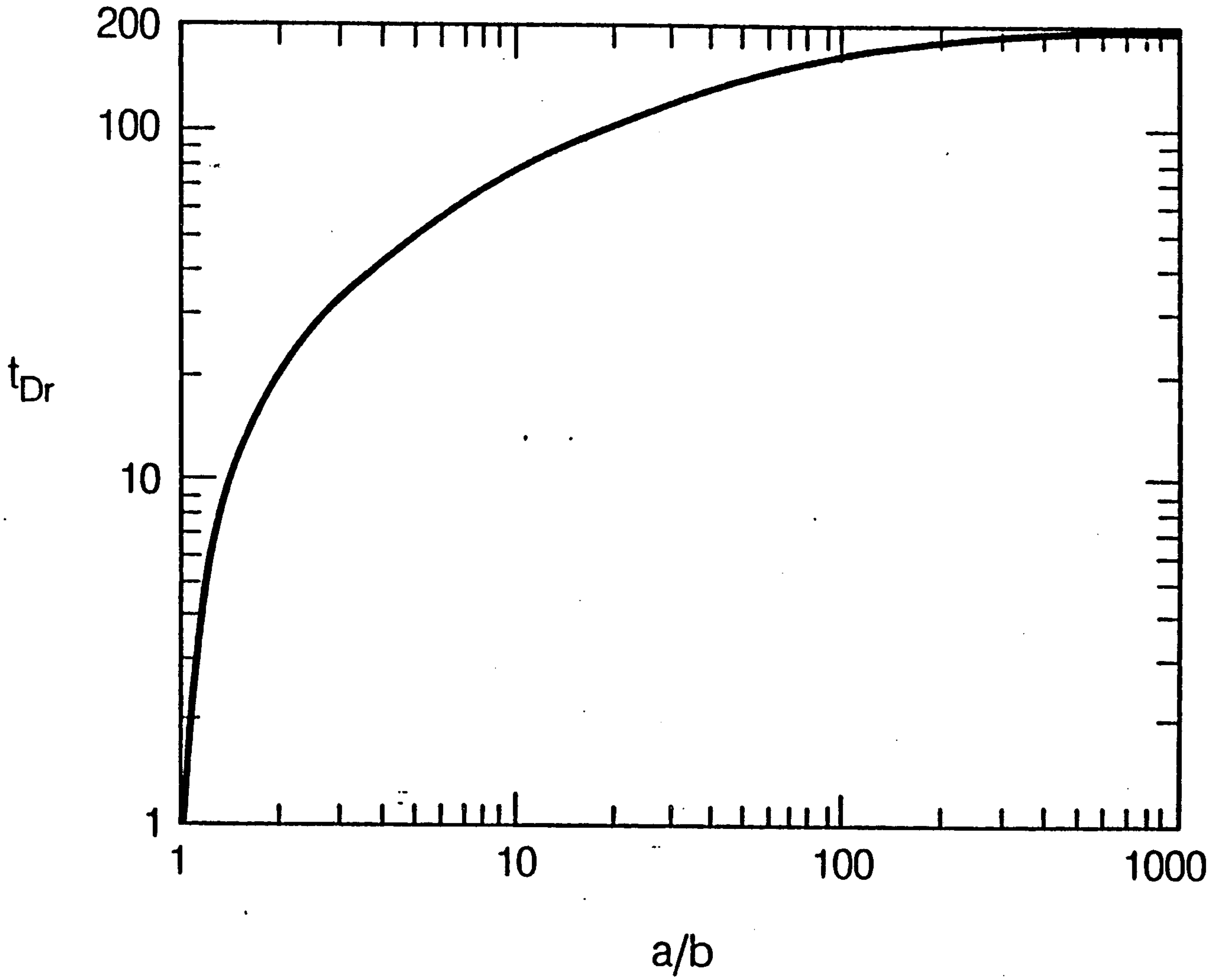

XBL 869-11004

Fig. 2. Dimensionless times for the onset of radial flow in elliptical flow systems (after Kucuk, 1978).

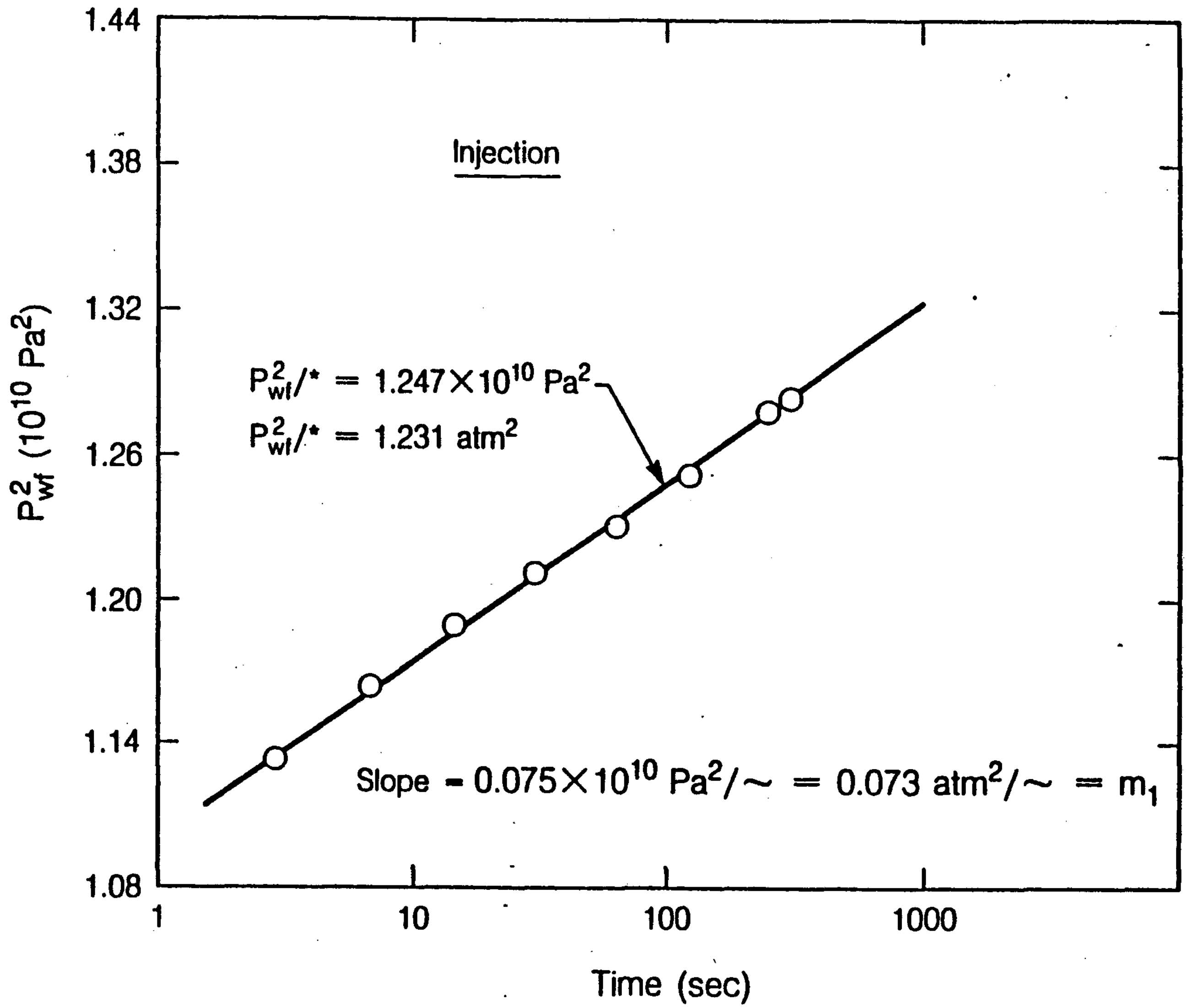

XBL 869-11007

Fig. 3. Semi-log graph of air injection test pressure response.

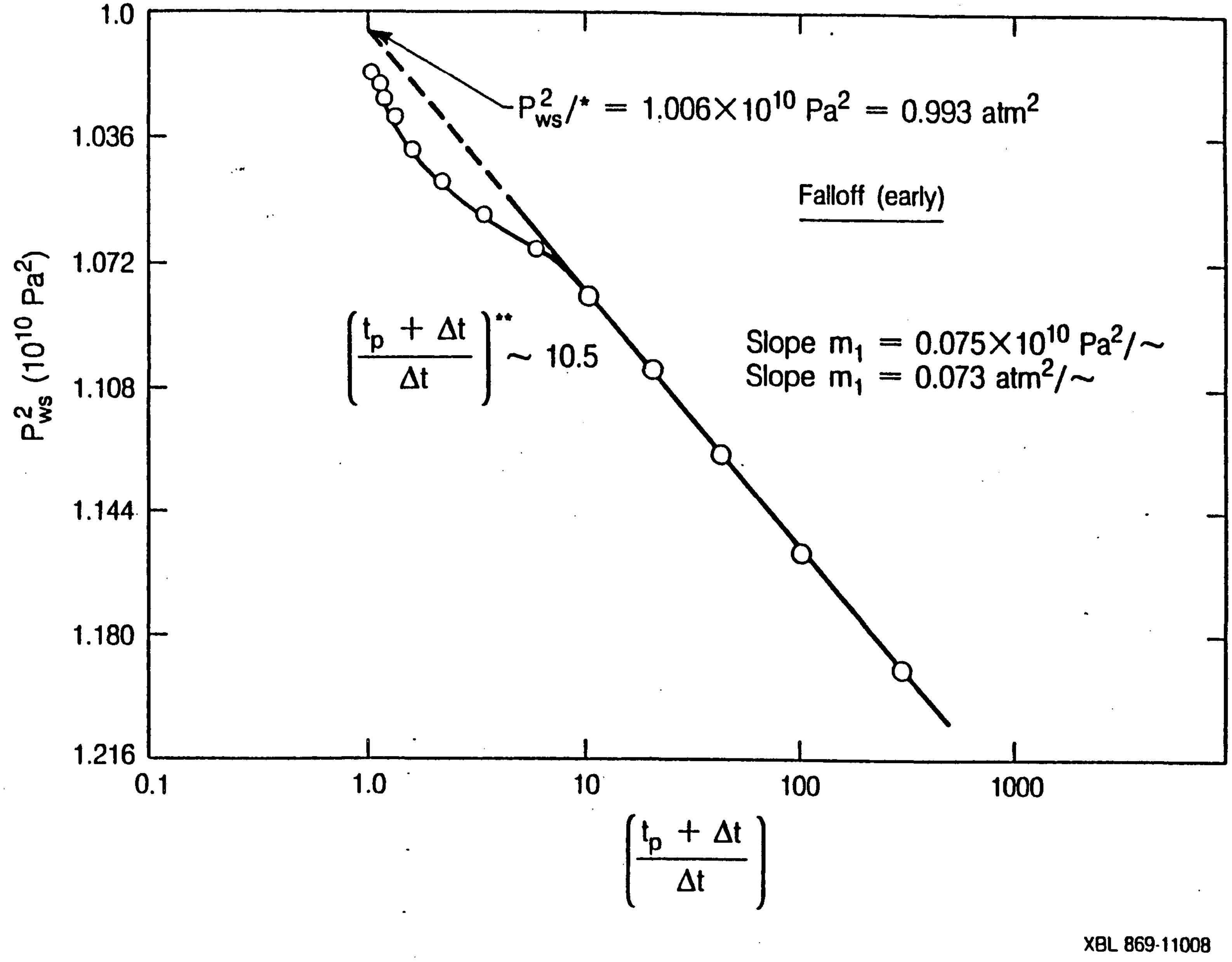

Fig. 4. Horner graph of early-time pressure falloff data - air injection.

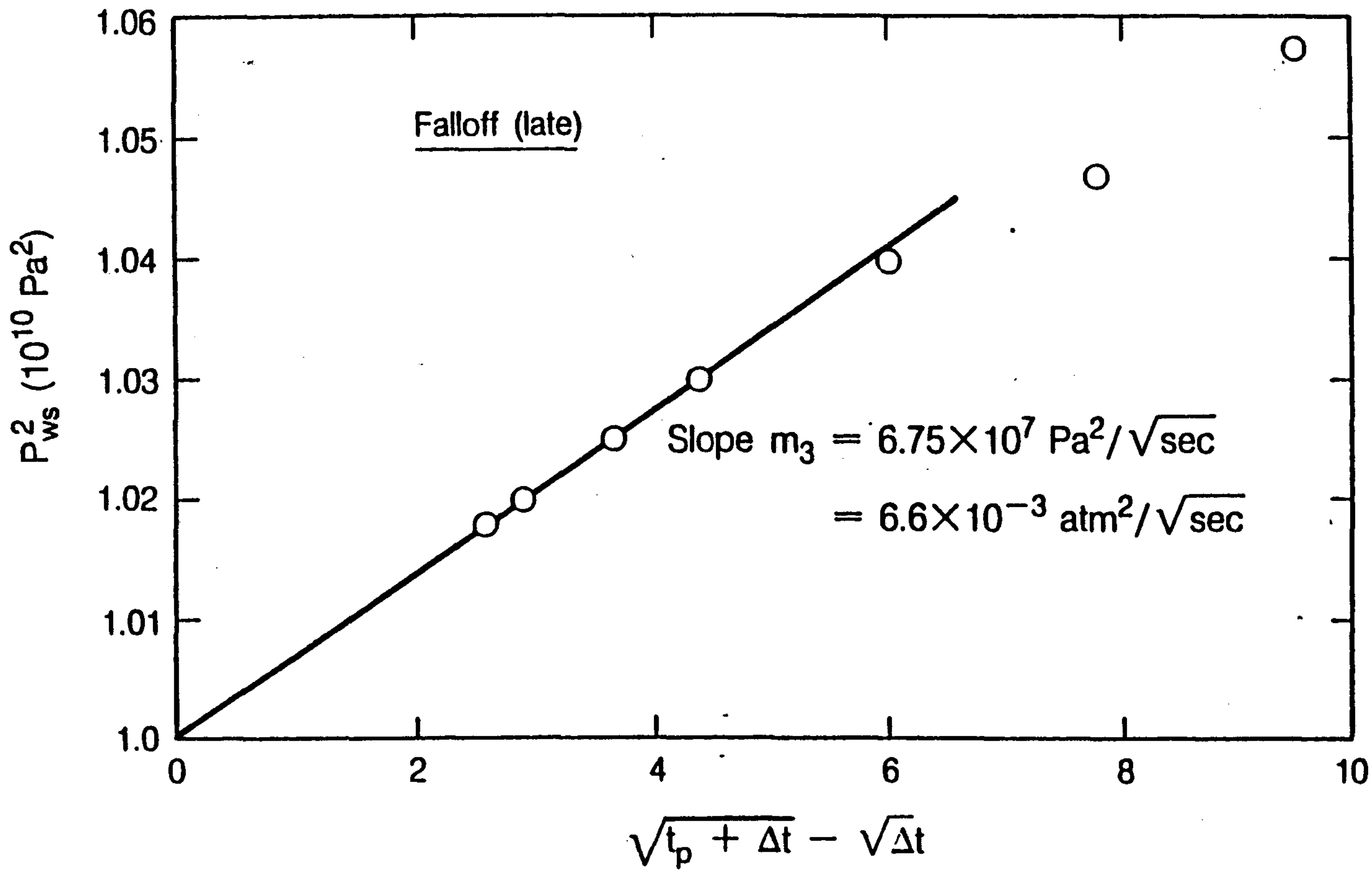

XBL 869-11009

Fig. 5. Square-root of time graph for late-time falloff pressure data - air injection.

LAWRENCE BERKELEY LABORATORY
TECHNICAL INFORMATION DEPARTMENT
UNIVERSITY OF CALIFORNIA
BERKELEY, CALIFORNIA 94720